Radical *para*-Benzoic Acid Derivatives: Transmission of Ferromagnetic Interactions through Hydrogen Bonds at Long Distances

Daniel Maspoch,[a] Laure Catala,[a] Philippe Gerbier,[b] Daniel Ruiz-Molina,[a] José Vidal-Gancedo,[a] Klaus Wurst,[c] Concepció Rovira,[a] and Jaume Veciana*[a]

Abstract: Investigation of the transmission of magnetic interactions through hydrogen bonds has been carried out for two different benzoic acid derivatives which bear either a *tert*-butyl nitroxide (NOA) or a poly(chloro)triphenylmethyl (PTMA) radical moiety. In the solid state, both radical acids formed dimer aggregates by the complementary association of two carboxylic groups though hydrogen bonding. This association ensured that atoms with most spin density are separated from one another by more than 15 Å. Thus, no competing through-space magnetic exchange interactions are expected in these dimers and, hence, they provide good models to investigate whether noncovalent hydrogen bonds play a role in the long-range transmission of magnetic interactions. The nature of the magnetic exchange interaction and their strengths within similar dimer aggregates in solution was assessed by electron spin resonance (ESR) spectroscopy. In the case of radical NOA, low-temperature ESR experiments showed a weak ferromagnetic interaction between the two radicals in the dimer aggregates (which have the same geometry as in the solid state). In contrast, the corresponding solution ESR study performed with radical PTMA did not lead to any conclusive results, as aggregates were formed by noncovalent interactions other than hydrogen bonds. However, the bulkiness of the poly(chloro)triphenylmethyl radical prevented interdimer contacts in the solid state between regions of high spin density. Hence, solid-state measurements of the α phase of PTMA radical provided evidence of the intradimer interaction to confirm the transmission of a weak ferromagnetic interaction through the carboxylic acid bridges, as found for the NOA radical. Moreover, crystallization of the PTMA radical in presence of ethanol to form the β phase of PTMA radical prevented the dimer formation; this resulted in the suppression of this interaction and provides further evidence of the magnetic exchange mechanism through noncovalent hydrogen bonds at long distances.

Keywords: dimerization · EPR spectroscopy · hydrogen bonds · radicals · through-bond interactions

Introduction

During the last decade, great interest has been focused on purely organic magnetic materials,[1] stimulated by the discovery of bulk ferromagnetism in α-nitronyl nitroxide derivatives at low temperatures.[2] Since ferromagnetism is a cooperative property, intermolecular magnetic interactions between the spin-bearing molecules must be controlled. Consequently, a well-designed purely organic magnetic material depends on two aspects: 1) the capacity to control the structural arrangement in the crystal and 2) the ability to predict the magnetic interactions that are associated with each arrangement. Crystal engineering through hydrogen bonds is a powerful method for achieving the first condition; that is, controlling the relative positioning of the neighboring molecules through the formation of well-defined supramolecular patterns in the solid state.[3] Nevertheless the role hydrogen bonds play in the transmission of magnetic interactions is still not completely understood. Several groups have taken advantage of this noncovalent approach in designing organic ferromagnets.[4–14] Most reported examples are based on α-nitronyl nitroxide, α-imino nitroxide, or *tert*-butyl nitroxide derivatives because of their high stability and the ability of their nitroxide (NO) groups to act as acceptors of hydrogen bonds. A strategy that has been used with these radicals combines the nitroxide radical with a diamagnetic compound that bears an appropriate hydrogen-bond donor group for the formation of hydrogen-bonded networks.[4, 5] Nevertheless,

[a] Prof. J. Veciana, D. Maspoch, Dr. L. Catala, Dr. D. Ruiz-Molina, Dr. J. Vidal-Gancedo, Dr. C. Rovira
Institut de Ciència de Materials de Barcelona (CSIC)
Campus Universitari de Bellaterra, 08193 Cerdanyola (Spain)
Fax: (+34) 393-580-5729
E-mail: vecianaj@icmab.es

[b] Dr. P. Gerbier
Laboratoire de Chimie Moléculaire et Organisation du Solide
UMR-5637, Université Montpellier 2, Place E. Bataillon
34095 Montpellier (France)

[c] Dr. K. Wurst
Institut für Allgemeine Anorganische und Theoretische Chemie
Universität Innsbrück, 6020, Innrain 52a (Austria)

 © 2002 WILEY-VCH Verlag GmbH & Co. KGaA, Weinheim 0947-6539/02/0816-3635 $ 20.00+.50/0

this strategy leads to a dilution of the magnetically active units in the solid and, therefore, to an increase of their separation, which in turn decreases the strength of intermolecular magnetic interactions. To avoid such drawbacks, the hydrogen-bond donor groups can be directly introduced on the molecule that bears the radical, so that self-assembled patterns can be formed directly between the paramagnetic molecules. An alternative approach is to use magnetically active transition metal ions as hydrogen-bond acceptor species and those radicals as ligands. These approaches have been successfully applied to nitroxide radicals with various substituents such as phenol,[6] boronic acid,[7] imidazole,[8] benzimidazole,[8, 9] triazole,[10] uracil,[11] pyrazole,[12] phenyl acetylene,[13] or benzoic acid.[14, 16–19] Besides their structural control, hydrogen bonds have also been shown to favor magnetic exchange interactions between bound radical molecules. Thus, in the solid state, a few examples have illustrated the propagation of magnetic exchange through strong (OH···O) and weak ($CH_3 \cdots O$) hydrogen bonds.[4, 6] Furthermore, polarized neutron diffraction experiments, which were performed on an α-nitronyl nitroxide acetylenic derivative, have provided an example in which spin density is transferred through the covalent framework from the NO group to a H atom on a ethynyl group, which is involved in a intermolecular hydrogen bond.[13] With the design of radical molecules that bear hydrogen-bond donor and acceptor groups, the structural dimensionality of the material may be controlled to some extent and, hence, also the propagation of the magnetic interactions through the supramolecular structure. However, the difficulty lies in the determination of the strength and nature of the magnetic interaction through this supramolecular pathway, since many other intermolecular interactions compete in the solid state. An interesting way to avoid this complexity is to obtain oligomers (dimers, trimers, etc.) with well-defined geometries in solution, since such supramolecular entities are isolated from each other and, therefore, other types of intermolecular interactions would not be present.[6e, 11, 12, 17] The main problem in these supramolecular aggregates is that NO groups are often involved in hydrogen bonds and this gives rise to cyclic dimers or trimers with their regions of radical spin density quite close to one another. To find suitable radicals that form hydrogen-bonded supramolecular aggregates in solution and in which the radicals centers are far enough away for a direct through-space magnetic interaction, we designed the two open-shell *para*-benzoic acid derivatives that bear either a *tert*-butyl nitroxide group in the case of the radical NOA (**1**) or a polychlorinated triphenylmethyl radicalin the case the radical PTMA (**2**), as open-shell moieties. The general trend of carboxylic acids to form dimers,

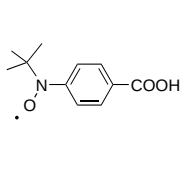

NOA (**1**)

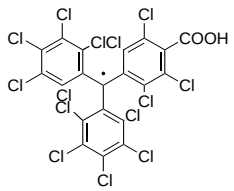

PTMA (**2**)

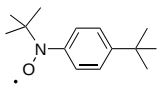

NO*t*Bu

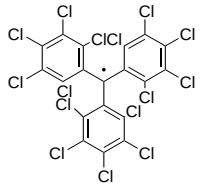

PTMCl

both in solution and in solid state,[15] suggested that both radicals would be ideal systems to show whether the propagation of the magnetic exchange is efficient at a long distance. Indeed, the ring pattern that they may form through the two complementary carboxylic groups could prevent the atoms with most of the radical spin density from approaching each other. These compounds provide a good model for the study of the magnetic exchange interaction through noncovalent hydrogen bonds without perturbations from direct

Abstract in Catalan: *La investigació de les transmissions d'interacció magnètica s'ha portat a terme utilitzant dos derivats diferents d'àcid benzoic, més concretament les espècies radicalàries nitròxid tert-butílic (NOA) i policlorotrifenilmetil (PTMA). En ambdós radicals, s'han observat agregats dimèrics en estat sòlid, formats per l'associació complementària dels grups carboxílics mitjançant enllaços d'hidrogen. Aquesta associació assegura que els àtoms amb major densitat d'espí estiguin allunyats amb distàncies més llargues que 15 Å els uns respecte als altres. Aquest fet origina que en aquests dímers no s'esperin altres interaccions d'intercanvi magnètic a través de l'espai, essent bons models per observar quin paper juguen els enllaços d'hidrogen en la transmissió d'interaccions magnètiques a distàncies llargues. Un altre camí per determinar la naturalesa i força de les interaccions d'intercanvi magnètic era estudiar la mateixa classe d'agregats en solució mitjançant l'espectroscòpia de RPE. En el cas del radical NOA, experiments de RPE a temperatura baixa van evidenciar la presència d'interaccions ferromagnètiques dèbils entre els dos radicals dels agregats dimèrics, els quals tenen la mateixa geometria que en estat sòlid. A diferència, estudis similars de RPE amb el radical PTMA no van portar a cap conclusió, degut a que en solució es formaven altres agregats no covalents a més dels de naturalesa d'enllaços d'hidrogen. No obstant, degut a la grandària dels radicals policlorotrifenilmetílics, es van negligir els contactes entre regions on la densitat d'espí és més elevada entre diferents dímers en estat sòlid. Així, les mesures del radical PTMA (fase alfa) en estat sòlid van aportar evidències clares sobre la interacció a dins d'un dímer, la qual va confirmar la transmissió d'interaccions ferromagnètiques dèbils a través de ponts d'àcid carboxílic, a l'igual que en el radical NOA. A més, la cristallització del radical PTMA en presència d'EtOH, que dóna lloc a la fase β del radical PTMA, preveu la formació dels dímers, suprimint així aquesta interacció i donant més evidències del mecanisme d'intercanvi magnètic mitjançant enllaços d'hidrogen no covalents a distàncies llargues.*

 © 2002 WILEY-VCH Verlag GmbH & Co. KGaA, Weinheim 0947-6539/02/0816-3636 $ 20.00+.50/0 *Chem. Eur. J.* **2002**, *8*, No. 16

through-space interactions. We describe herein the synthesis and extensive magnetic studies, both in solution and in the solid state, of these two radicals and show that magnetic exchange interactions are transmitted efficiently through the hydrogen bonds that form between the two COOH groups.

Results and Discussion

Synthesis: Radical NOA was synthesized by a three-step procedure from 1-[*N*-*tert*-butyl-*N*-(*tert*-butyldimethylsiloxy)amino]-4-bromobenzene (**3**),[20] as shown in Scheme 1. The carboxylic acid function was introduced by the reaction of the lithiated derivative **4** with CO_2 and then the removal of the protecting group with fluoride ions. The oxidation of the hydroxylamine **5** by PbO_2 afforded the NOA radical (**1**) as a crystalline red-orange solid. Red-orange needle-shaped crystals were obtained by crystallization from dichloromethane. PTMA (**2**) was synthesized according to the procedure described in the literature.[20] The crystallization of this radical was performed by diffusion of hexane into a dichloromethane solution of the radical to form the α phase as red thin plates. This crystalline phase is a clathrate compound that contains two molecules of dichloromethane in the unit cell. The β phase was formed as red needles by slow evaporation of a solution of the radical from EtOH. This phase is also a clathrate compound that contains three molecules of ethanol to two radicals.

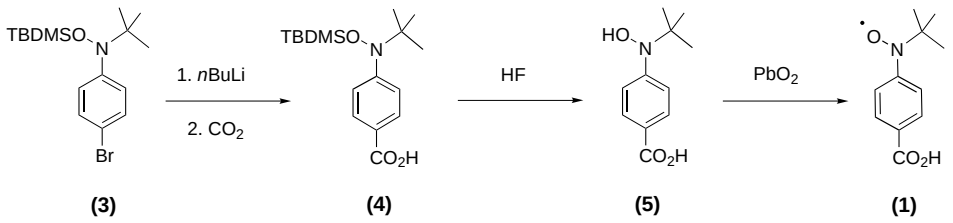

(3) (4) (5) (1)

Scheme 1. Synthesis of the NOA radical.

Crystal structures: Radical NOA crystallizes in the $P2_1/n$ monoclinic space group and the cell parameters are reported in Table 1. The asymmetric unit (Figure 1a) has a conformation in which the torsion angle between the benzene ring and the carboxylic group is 3.8°. The normal to the plane defined by the $C_{ar}NO$ atoms makes an angle of 18.3° with the normal to the phenyl ring. This value is well within the range of crystallographic values for related molecules. Thus, this radical adopts a nearly planar conformation, which seems to be favored by the weak intramolecular hydrogen bonds between the aromatic H atoms and the O atoms of carboxylic acid (O2···HC4, 2.51 Å; C4-H-O, 98°) and the NO groups (O3···HC3, 2.37 Å; C3-H-O, 99°). In most of dimers previously reported for other carboxylic acids, the C=O and C–OH atoms are often disordered,[22] and this gives rise to apparent equivalent C–O bond lengths. However, in this case, two nonequivalent C–O bonds are found (C8–O2, 1.237(2) Å and C8–O3, 1.302(2) Å). These bond lengths correspond to the C=O and C–OH bonds, respectively. Again, this feature seems to be due to the weak intramolecular hydrogen bonds which lock the oxygen of the C=O group in the O2 rather than the O3 position.

Table 1. Crystallographic parameters of NOA and PTMA radicals.

	NOA	PTMA (α phase)	PTMA (β phase)
formula	$C_{11}H_{14}N\,O_3$	$C_{20.5}H_2Cl_{15}O_2$	$C_{23}H_{10}Cl_{14}O_{3.50}$
M_r	208.23	811.97	838.61
lattice type	monoclinic	Triclinic	Triclinic
space group	$P2_1/n$	$P\bar{1}$	$P\bar{1}$
a [Å]	6.8949(5)	8.8400(3)	8.816(2)
b [Å]	8.7147(3)	12.8188(5)	13.840(4)
c [Å]	18.377(1)	14.3719(6)	14.379(5)
α [°]	90	96.461(2)	66.645(8)
β [°]	92.427(2)	97.378(2)	79.87(2)
γ [°]	90	98.607(2)	88.20(2)
V [Å^3]	1103.23(11)	1582.44(11)	1584.2(8)
Z	4	2	2
ρ_{calcd} [g cm^{-3}]	1.254	1.704	1.758
T [K]	218	223	223
reflections measured	1626	4665	2138
reflections observed [$I > 2\sigma(I)$]	1355	4058	1474
$R1$ [$I > 2\sigma(I)$]	0.0374	0.0494	0.0743
$R1$ (all data)	0.0466	0.0605	0.1159
$wR2$ (all data)	0.1023	0.1852	0.1846

Complementary hydrogen bonding between the two carboxylic groups of neighboring radicals (O2···HO3, 1.64 Å; O2-H-O3, 176°) generated, as the *primary crystalline pattern*, the hydrogen-bonded dimers shown in Figure 2a. The eight-membered ring formed by the hydrogen-bonded carboxylic acid fragments lies in the plane of the benzene rings as the torsion angle between the carboxylic group and the benzene ring is small. The molecules that are related by the inversion center of the unit cell are $\pi-\pi$ stacked with a distance of 3.66 Å between the aromatic rings. Furthermore, the molecules are also related along the *a* axis by two sets of weak hydrogen bonds that involve an aromatic H atom of one molecule and the NO (O1···HC3, 2.65 Å; C3-H-O, 134°) and carboxylic groups (O3···HC6, 2.57 Å; C6-H-O, 135°) of neighboring molecules. These contacts connect the dimers together into distinct layers, A and A′, within the *ab* plane; this constitutes the *secondary crystalline pattern* (Figure 2b). Layers A and A′ are further connected along the *c* direction by two weak hydrogen bonds between the *tert*-butyl and carboxylic groups of one molecule (O2···HC12, 2.60 Å; C12-H-O2, 170°) and the NO group (O1···HC13, 2.81 Å; C13-H-O1, 160°) of the neighboring molecule. Finally, the long separation of the two NO groups within the dimers is notable (15.15 Å), while the shortest contact between NO groups is 6.08 Å between the N atoms of the $\pi-\pi$ stacked molecules.

As already mentioned, radical PTMA crystallizes in two polymorphs, α and β, which depend on the crystallization conditions. The α phase crystallizes in the $P\bar{1}$ triclinic space group and the cell parameters are reported in Table 1. A molecule of dichloromethane is included in the cell with the

 © 2002 WILEY-VCH Verlag GmbH & Co. KGaA, Weinheim 0947-6539/02/0816-3637 $ 20.00+.50/0

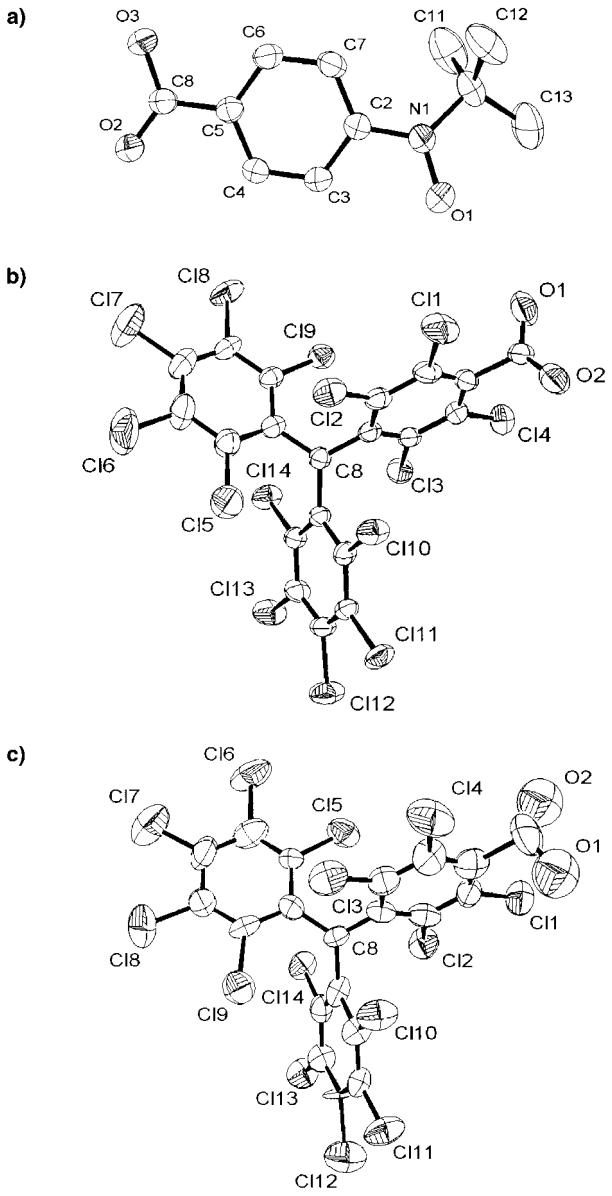

Figure 1. ORTEP representations of molecules found in a) radical NOA, b) the α phase of radical PTMA, and c) the β phase of radical PTMA in which the two carboxylic groups are present with a probability factor of 0.5.

PTMA radical in a 2:1 ratio. This clathrate compound is stabilized by a short Cl$\cdots$Cl contact (Cl15$\cdots$Cl9, 3.44 Å). In contrast to the NOA radical, the carboxylic group is disordered as two equivalent C–O bond lengths (C–O1, 1.218(6) Å and C–O2, 1.230(6) Å) are found. The absence of any stabilization of the C=O bond in one position by the weak hydrogen bonds accounts for this difference. The torsion angles between the mean planes of the three polychlorinated aromatic rings and that of the three bridgehead and one methyl C atoms (the reference plane) are 46, 51, and 55°. These angles generate the propeller-shape conformation which is usually found in this family of radicals (Figure 3a).[23] Due to the steric hindrance from the chlorine atoms *ortho* to the carboxylic group, the carboxylate is twisted by 88° with respect to the phenyl plane to which it is bonded. The primary crystalline pattern of the α phase is also a hydrogen-bonded

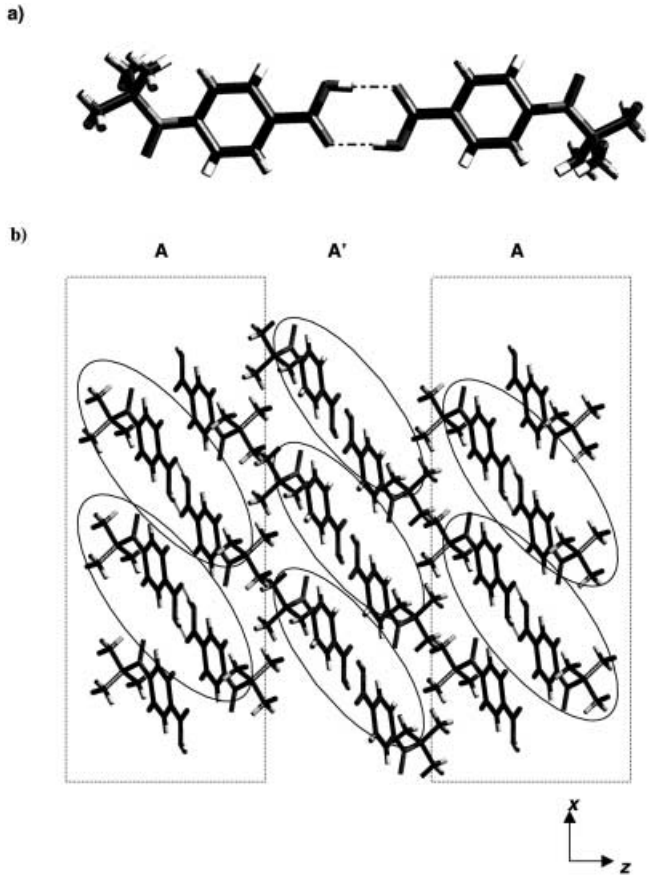

Figure 2. a) View of the hydrogen-bonded dimer formed by radical NOA in the solid state b) View along the *b* axis of the primary and the secondary crystalline patterns.

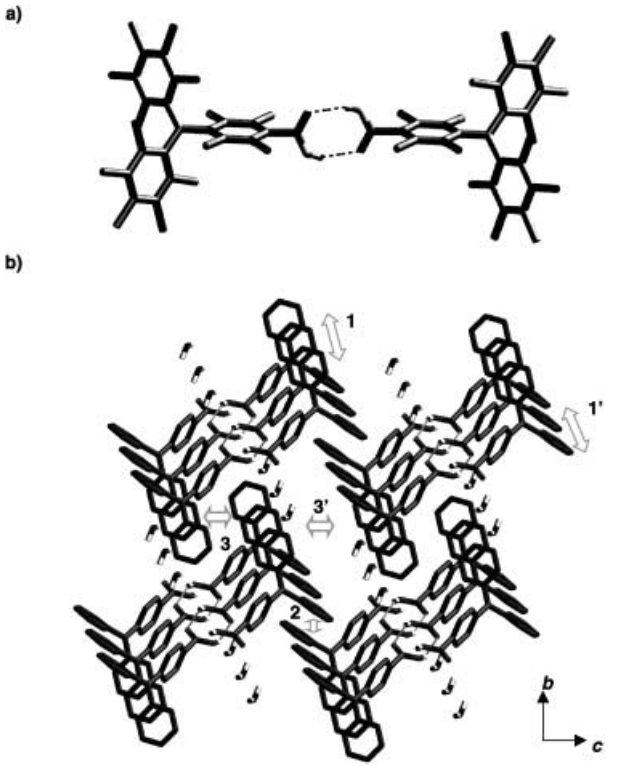

Figure 3. a) View of hydrogen-bonded dimer in the α phase of radical PTMA. b) Representation along the *a* axis of the shortest contacts in the molecular packing of α phase of PTMA.

© 2002 WILEY-VCH Verlag GmbH & Co. KGaA, Weinheim
0947-6539/02/0816-3638 $ 20.00+.50/0 *Chem. Eur. J.* **2002**, *8*, No. 16

dimer formed through the two carboxylic groups (O1 ··· H-O2, 1.955 Å; O1-H-O2, 144°), as shown in Figure 3a. These dimers are connected to each other through short Cl ··· Cl contacts, as shown in Figure 3b. In the *a* direction there are two such contacts (1 and 1′: Cl(9) ··· Cl(1), 3.35 Å; Cl(10) ··· Cl(13), 3.40 Å, respectively), whereas only one contact is present in the *b* direction (2: Cl(4) ··· Cl(7), 3.46 Å) and two further contacts in the *c* direction are observed (3 and 3′: Cl(2) ··· Cl(8), 3.33 Å; Cl(5) ··· Cl(5), 3.22 Å, respectively). The shortest distance between the methyl C atoms of neighboring radicals is found within the dimers at a length of 15.36 Å.

In the β phase of radical PTMA, molecules crystallize in the $P\bar{1}$ triclinic space group and cell parameters are given in Table 1. The PTMA molecules also adopt a propeller-shape conformation with torsion angles of 45, 51, and 54° between the mean planes of the aromatic rings and the reference plane. The carboxylic acid group in this phase has an angle of around 89° with respect to the aromatic plane and is disordered with a 0.5 occupancy factor for the C12 and C2 atoms. This is shown on the ORTEP view (Figure 1c). There are ethanol molecules in the unit cell in a 1.5:1 ratio with PTMA and these form three different hydrogen bonds with the carboxylic acid (hydrogen bond 1: O2 ··· H-O5, 2.39 Å; O2-H-O5, 109°; hydrogen bond 2: O1 ··· H-O6, 2.52 Å; O1-H-O6, 124°; and hydrogen bond 3: O6 ··· H-O1, 2.37 Å; O6-H-O1, 139°). There is also an additional hydrogen bond between two of the EtOH molecules (hydrogen bond **4**: O5 ··· H-O6, 2.12 Å; O5-H-O6 142°). By bonding to the carboxylic group, EtOH prevents the formation of the dimer aggregates of PTMA that are found in the α phase. Thus, the primary crystalline pattern of the β phase consists of two molecules of PTMA with three molecules of EtOH in between them, as shown in Figure 4a. These patterns are related to each other by short Cl ··· Cl contacts. In the *a* direction, two of such contacts are present (1 and 1′: Cl5 ··· Cl4, 3.43 Å; Cl10 ··· Cl13, 3.42 Å), whereas only one such contacts is present in the *b* direction (2: Cl2 ··· Cl11, 3.46 Å) and two others in the *c* direction (3 and 3′: Cl14 ··· Cl8, 3.39 Å; Cl5 · · · Cl5, 3.22 Å).

Magnetic characterization—ESR solution studies: To get an overview of the unpaired electron delocalization on NOA and PTMA radicals, as well as to study the supramolecular aggregation they undergo in solution, X-band ESR spectra of dilute fluid and rigid (frozen) solutions were recorded under different experimental conditions.

Radical NOA: The room-temperature spectrum of NOA at a concentration of 1.0×10^{-4} M in dichloromethane consists of three overlapped groups of lines with 1:1:1 intensities, due to the hyperfine coupling of the unpaired electron with the nuclear spin of the N atom (Figure 5). The further splitting of each of these groups of lines arises from the additional coupling of the unpaired spin with the four H nuclei from the aromatic ring (two equivalent *ortho* H and two equivalent *meta* H nuclei). The coupling with the nine equivalent H atoms of the *t*Bu group is unresolved under these conditions. The whole spectrum can be simulated with the isotropic hyperfine coupling constants shown in Table 2; the simulated

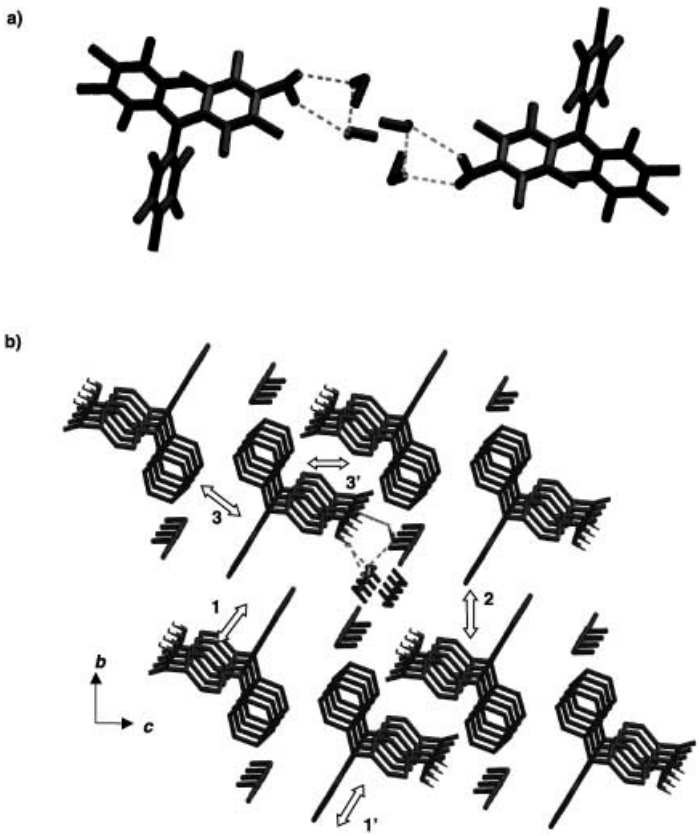

Figure 4. a) View of hydrogen-bonded dimer in the β phase of radical PTMA. The central EtOH molecules are disordered in the two depicted positions. b) Representation along the *a* axis of the shortest contacts in the molecular packing of β phase of PTMA.

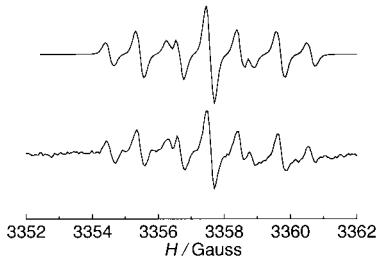

Figure 5. ESR spectra of NOA in a dilute dichloromethane solution at room temperature. Bottom: experimental spectrum: frequency: 9.392353 GHz; power: 5.090 W; modulation amplitude 0.2 G. The intensities of the two starred lines change with temperature and concentration (see text). Top: simulation of the spectrum, parameters in Table 2.

Table 2. Hyperfine coupling constants from simulation of ESR spectra of dilute solutions of radicals NOA and PTMA.

	Concentration [M]	a_N [Gauss]	$a_{H\text{-}ortho}$ [Gauss]	$a_{H\text{-}meta}$ [Gauss]	$a_{C\text{-}methyl}$ [Gauss]	$a_{C\text{-}ortho}$ [Gauss]	$a_{C\text{-}bridgehead}$ [Gauss]
NOA[a]	1.0×10^{-4}	11.57	2.13	0.92	–	–	–
NOA[b,d]	5.3×10^{-3}	11.00	2.30	0.92	–	–	–
		5.50	1.15	0.46			
NO*t*Bu[b]	5.3×10^{-3}	12.50	2.14	0.92	–	–	–
PTMA[c]	1.0×10^{-4}	–	–	–	30.0	13.1	10.7
PTMA[b]	1.0×10^{-4}	–	–	–	29.5	12.9	10.6
PTMCl[b]	5.3×10^{-3}	–	–	–	29.5	12.9	10.5

[a] Performed in CH_2Cl_2 at room temperature. [b] Performed in CH_2Cl_2/toluene (1:1) at 200 K. [c] Performed in CH_2Cl_2/toluene (1:1) at room temperature. [d] Biradical:radical molar ratio was of 3.1:1.0.

 © 2002 WILEY-VCH Verlag GmbH & Co. KGaA, Weinheim 0947-6539/02/0816-3639 $ 20.00+.50/0

spectrum is shown on the top of Figure 5. An interesting observation is the slight decrease in the hyperfine coupling of the N atom in radical NOA with respect to that of the *para tert*-butyl benzene derivative, NO*t*Bu, which was obtained under similar experimental conditions. This indicates that the unpaired electron is somewhat more delocalized on the aromatic ring of the radical NOA than in NO*t*Bu, due to the conjugation effect of the carboxylic group.[24, 25] The spectrum of radical NOA varies significantly as the radical concentration and the temperature are changed; additional lines appear at intermediate positions (starred in Figure 6) and increase in

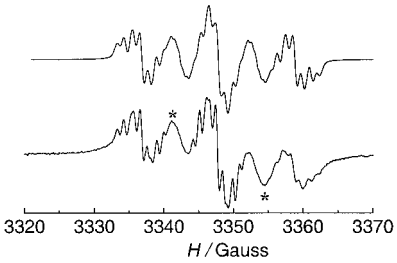

Figure 6. ESR spectrum of dilute solution of NOA in toluene/dichloromethane at 180 K. Concentration: 5.3×10^{-3} M; frequency: 9.395658 GHz; power: 1.016×10^{-1} mW; modulation amplitude: 0.403 G.

intensity as the temperature is lowered or the concentration is increased. These changes are reversible and indicate the formation of other paramagnetic species due to an aggregation phenomenon; that is, the establishment of equilibrium between radical molecules and supramolecular aggregates that can be shifted towards the aggregates when temperature is lowered or the concentration increased. The nature of these aggregates was investigated with a 5.3×10^{-3} M solution of NOA in dichloromethane/toluene (1:1 v/v). As shown in Figure 6, the experimental spectrum at 180 K is reproduced by the addition of the simulated spectrum of the monoradical with that of a dimer in a molar ratio of 1:3. For the simulation of the dimer, half the values of hyperfine coupling constants, a_N and a_H, of the monoradical and its g factor were used. Besides the dimeric nature of the aggregates, this result suggested that the two unpaired electrons of the dimer interact magnetically within the so-called "strong exchange limit" so that the exchange coupling constant J is much greater than a_N.[25b, 26] The dimeric nature of aggregates was further confirmed by the spectrum of the frozen solution, since both the fine structure and the half-field signal characteristic of a triplet species ($S = 1$) were observed (vide infra).

In principle, dimers of NOA may have several different geometries that depend on the nature and strength of the different interactions ($\pi - \pi$, strong and weak hydrogen bonds, etc.) which join the two radical moieties. Regardless of the nature and strength of these interactions, aggregates must be favored by increased radical concentration, so that above a certain concentration level, several kinds of aggregates may coexist. To exclude all aggregates formed by weak interactions and to limit the study only to those linked by strong hydrogen bonds, that is, aggregates formed by strong nitroxide/acid or acid/acid hydrogen bonds (see Scheme 2), it

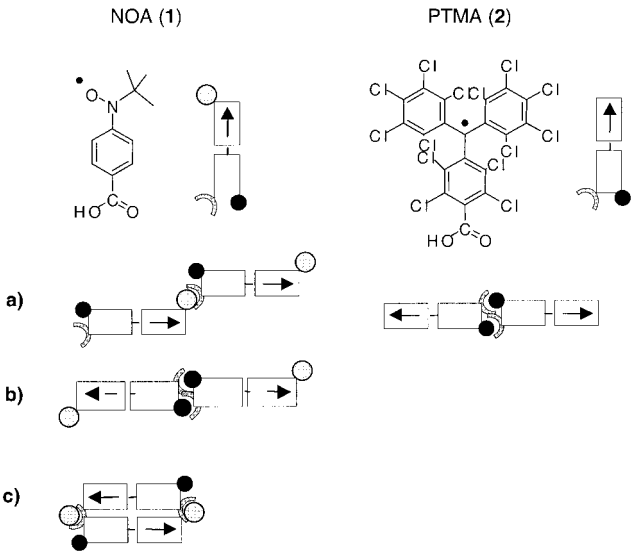

Scheme 2. Schematic representation of potential dimer aggregates which may form in solutions of NOA and PTMA radicals.

was important to determine the critical concentration below which only strong hydrogen bonds occur. We used the radical NO*t*Bu,[24] as a reference molecule, as it cannot be involved in any strong hydrogen-bond interactions and undergoes aggregation through other weak interactions. The spectrum of a 5.3×10^{-2} M solution of radical NO*t*Bu in dichloromethane/toluene (1:1 v/v) did not show any intermediate lines at room temperature; this suggested the unique presence of monomeric radicals. However, the frozen solution exhibited a half-field signal, which revealed that other kinds of aggregates form in solution. The solution was diluted to a value of 5.3×10^{-3} M, which ensured the absence of the half-field signal even at low temperatures and showed that aggregation phenomenon did not take place. Consequently, this concentration was adopted as the higher concentration limit for the study of the hydrogen-bonded dimers of NOA. Figure 7 shows the ESR spectrum of a frozen solution of NOA at 106 K at a concentration of 5.3×10^{-3} M in dichloromethane/toluene (1:1 v/v), in which the fine structure and half-field signal, which correspond to the $\Delta m_S = \pm 1$ and $\Delta m_S = \pm 2$ transitions of a triplet species ($S = 1$), respectively, are clearly observed. The presence of hydrogen bonds in such triplet species was confirmed by adding EtOH to the solution, which suppressed the half-field signal and gave a completely different $\Delta m_S = \pm 1$ signal, which was simulated with the parameters from Table 3, and which corresponds to a randomly oriented ensemble of monomeric radicals.

As shown in Scheme 2, dimer aggregates which are linked by strong hydrogen bonds may have either a linear or a cyclic geometry. In the first case the two radical moieties could be joined either by a single nitroxide/acid hydrogen bond (aggregate **a**) or by two complementary acid/acid hydrogen bonds (aggregate **b**), whereas in the cyclic case the radicals would be joined by two complementary nitroxide/acid hydrogen bonds (aggregate **c**). At first glance, aggregate **a** seems improbable, since the two other alternatives are energetically more favored by the formation of two hydrogen bonds instead

© 2002 WILEY-VCH Verlag GmbH & Co. KGaA, Weinheim
0947-6539/02/0816-3640 $ 20.00+.50/0 *Chem. Eur. J.* **2002**, *8*, No. 16

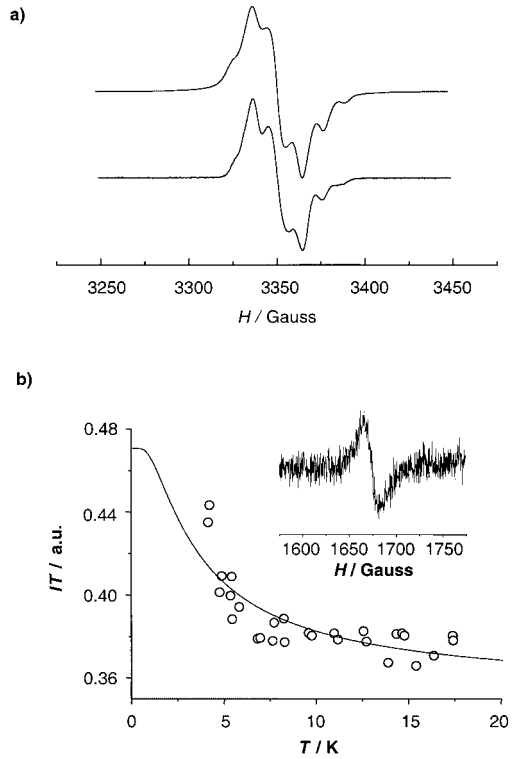

Figure 7. a) Experimental $\Delta m_S = \pm 1$ signal of NOA at 109 K (bottom). Concentration: 5.3 ± 10^{-3} M; frequency: 9.405598 GHz; power: 1.016×10^{-1} mW; modulation amplitude: 0.403 G. Simulated signal (top), parameters in Table 3. b) Temperature dependence of the peak–peak intensity, I_{pp}, plotted as $I_{pp}T$ product versus T, which corresponds to the $\Delta m_S = \pm 2$ transition. The solid line is the best fit of the experimental data to the Bleaney–Bowers equation. Inset: Observed $\Delta m_S = \pm 2$ signal at 109 K.

Table 3. ESR parameters used for the simulation of $\Delta m_S = \pm 1$ signals of monoradical and diradical aggregates of NOA in solution at 106 K.

Species	Components of $\boldsymbol{g}$ tensor	Components of $\boldsymbol{A}$ tensor[c]	D' [Gauss]	E' [Gauss]	B_{pp} [Gauss]
monoradical[a]	$g_{xx} = 2.0070$	$A_{xx} = 4.2$	–	–	$B_x = 8$
	$g_{yy} = 2.0070$	$A_{yy} = 4.2$			$B_y = 8$
	$g_{zz} = 2.0022$	$A_{zz} = 26.3$			$B_z = 9$
diradical[b]	$g_{xx} = 2.0070$	$A_{xx} = 2.1$	6.5 ± 1	0.0	$B_x = 15$
	$g_{yy} = 2.0070$	$A_{yy} = 2.1$			$B_y = 15$
	$g_{zz} = 2.0022$	$A_{zz} = 13.0$			$B_z = 3.5$

[a] In a 1:1 dichloromethane/toluene mixture with 3% of EtOH. [b] In a 1:1 dichloromethane/toluene mixture. [c] Components of the hyperfine coupling tensor with the N nuclei, assuming that $\boldsymbol{A}$ and $\boldsymbol{g}$ tensors are colinear.

of one. The most probable aggregates, diradicals **b** and **c**, can be distinguished by their zero-field-splitting (ZFS) parameters D' and E'. D' is related to the effective interspin distance, r, which can be calculated from the distance between the spin-bearing sites in the point dipole approximation by $D' = 27887/r^3$, in which D' is given in Gauss and r in Å. In contrast, the E' parameter simply relates to the symmetry of the diradical. Assuming that the spin density of aggregates **b** and **c** is mostly localized in two points around the two NO groups, r will be approximately twice the length for linear aggregate **b** than for cyclic **c**; therefore, the value of D' will be very different in both types of aggregates.

Hence, from the D' value, obtained from the simulation of experimental spectrum (see Table 3), a value of $r = 16.2$ Å was determined for the dimer aggregates present in solution. This value is close to the separation of the N and O atoms ($r_{N-N} = 15.1$ Å and $r_{O-O} = 16.4$ Å) determined in the solid state for the **b**-type dimers. Alternatively, if type **c** aggregates were formed, the separation would be less than 8 Å; hence this hypothesis must be discarded. Another estimate of r of the of NOA radical aggregates can be obtained from the relative intensity of the signal of the half-field transition, $I(\Delta m_s = \pm 2)$, to the signal, $I(\Delta m_s = \pm 1)$, of the allowed transition, since such a relative intensity is directly proportional to r^{-6}.[27] The proportionality constant depends on the nature of radical center, but in the case of the nitroxyl radical, which has an r value of 9–12 Å, it has been determined by Dubinskii et al.[28] to be 38 Å^6. Hence, the relative intensity, $I(\Delta m_s = \pm 2)/I(\Delta m_s = \pm 1)$, is obtained by the integration of the signal after correction for the content of free monomer radical, and a distance of 14.9 Å was determined. This result confirmed that radical NOA forms aggregates of type **b** in solution.

Another important aim of this study was to determine the nature and the strength of the magnetic exchange interactions that propagate within the aggregates through the hydrogen bonds at a long distance. To do so, the temperature dependence of the peak-to-peak intensity (I_{pp}) of the half-field signal was determined in the 4–100 K temperature range. The $I_{pp}T$ product plotted against temperature (Figure 7b) revealed the presence of ferromagnetic interactions within the dimers and demonstrated that the triplet is the ground state. Finally, the strength of the interactions within the dimer was determined by fitting the temperature dependence of I_{pp} to the Bleaney–Bowers equation,[29] which gave a value for the exchange coupling constant $J/k_B = 2.0 \pm 0.5$ K (using the Hamiltonian $\mathcal{H} = -2J(S_A \cdot S_B)$). This result demonstrates the efficiency of the coupling through a hydrogen bond even at long distances by using strongly delocalized radicals. The mechanism of ferromagnetic interaction is not clear, but it could be explained by the spin polarization mechanism (Scheme 3) if a regular alternation of the spin density on all the nuclei of the dimer with a significant value on the two H nuclei of hydrogen-bonded CO_2H groups is assumed.

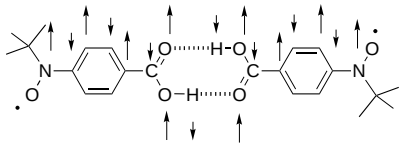

Scheme 3. Schematic representation of alternating spin densities in the hydrogen-bonded dimers of radical NOA.

Radical PTMA: The room-temperature ESR spectrum of radical PTMA in dichloromethane/hexane (1:1 v/v) shows one central main line surrounded by few weak satellite lines (Figure 8). These satellite lines originate from the hyperfine coupling of the unpaired electron with magnetically active ^{13}C nuclei in natural abundance at the α, bridgehead, and *ortho* positions. The experimental spectrum can be simulated by using the isotropic hyperfine coupling constants reported in

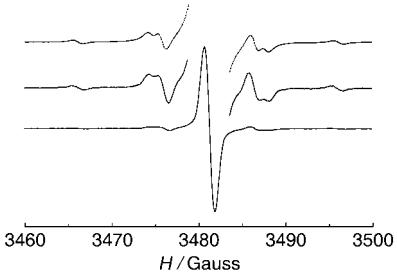

Figure 8. Experimental ESR spectrum (bottom) of a dilute solution of PTMA in toluene/dichloromethane (1:1 v/v) at room temperature. Concentration: 1×10^{-4} M; frequency: 9.756698 GHz; power: 5.090×10^{-1} mW; modulation amplitude: 1.0 G. Experimental spectrum (middle) in which the central line has been enlarged in order to observe the satellite lines. Simulated spectrum (top), parameters in Table 2.

Table 2; the simulated spectrum is shown in Figure 8. No significant differences were seen between the hyperfine coupling constants of this radical and that of radical PTMCl,[30] under similar experimental conditions; this indicates that the replacement of a Cl atom by a COOH group does not produce any noticeable change of the spin-density distribution.

To study the hydrogen-bonding aggregation phenomenon of radical PTMA in solution, the effect of concentration and temperature on the ESR spectra were studied for this radical and for reference radical PTMCl,[31]. ESR spectra, which were obtained at 111 K for solutions of the PTMCl radical of concentration 5.3×10^{-3} and 2.7×10^{-3} M in a dichloromethane/toluene (1:1 v/v), contained a significant half-field signal indicative of aggregate formation by interactions other than hydrogen-bonding. This tendency is specific to this family of compounds,[29] and may be explained by $Cl \cdots Cl$ and $\pi \cdots \pi$ interactions between aromatic rings of neighboring radicals, as these interactions are always present in their crystal structures. When the concentration of PTMCl was further lowered to 1.0×10^{-3} M, no half-field signals were detected; this suggests that at this critical concentration no aggregates were formed. This limiting concentration was thus used to study the aggregation of radical PTMA. However, at this concentration the spectrum of PTMA did not exhibit a half-field signal either, indicating that this concentration is also too low to induce hydrogen-bonded dimers. In contrast with NOA, no critical concentration was found in which only hydrogen-bonded dimers of PTMA were formed without the presence of other parasite aggregates.

To see if other information could be extracted about the size and nature of the aggregates, the ESR spectra of a concentrated solution of PTMA at 5.3×10^{-2} M was examined. The ESR spectrum in isotropic conditions (fluid solution) only showed the typical features of the monomer, although it is possible that the presence of exchange narrowed lines from dimers are hidden under the broad lines of monomer. In frozen solution (Figure 9), a signal from $\Delta m_S = \pm 1$ was observed as one weakly resolved line and there were no significant changes in comparison to the spectrum from dilute 1.0×10^{-3} M solution. Interestingly, a $\Delta m_S = \pm 2$ half-field signal was observed in the spectrum of the concentrated solution as a broad unresolved line. As a consequence, we may

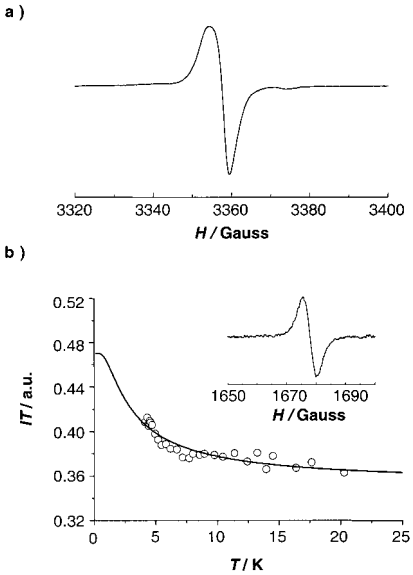

Figure 9. a) Experimental ESR $\Delta m_S = \pm 1$ signal of PTMA at 106 K. Concentration: 5.3×10^{-3} M in CH_2Cl_2/toluene; frequency: 9.406904 GHz; power: 3.212×10^{-2} mW; modulation amplitude: 0.5 G. b) Temperature dependence of the peak–peak intensity, I_{pp}, plotted as $I_{pp}T$ product versus T, which corresponds to the $\Delta m_S = \pm 2$ transition. The solid line is the best fit of the experimental data to the Bleaney–Bowers equation. Inset: Observed $\Delta m_S = \pm 2$ signal at 106 K.

confirm the presence of aggregates in concentrated solutions of radical PTMA, but this result does not permitan assessment of either the nature or the size of such aggregates due to the poorly resolved spectra.

Solid-state studies: The static magnetic susceptibility, χ, of polycrystalline samples of both α and β phases of PTMA as well as of radical NOA, was measured between 5 and 300 K with a SQUID susceptometer. At room temperature, the χT product values for all three samples agree with the theoretical value of 0.375 emu K^{-1} mol^{-1} for uncorrelated $S = 1/2$ moieties. The paramagnetic susceptibility χ of NOA, which is plotted as χT product in Figure 10, decreases when the

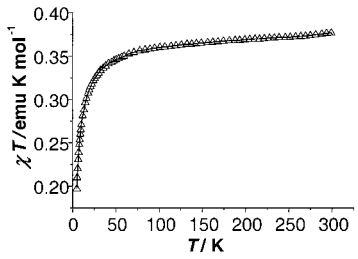

Figure 10. Temperature dependence of the magnetic susceptibility χ of polycrystalline sample of NOA which is plotted as χT versus T. Solid line is the best fit of the experimental data.

temperature is lowered below 50 K. This reveals the presence of dominant antiferromagnetic interactions at low temperature in the solid state. In the crystal structure, through-space contacts between NO groups that bear most of the spin density are longer than 6 Å; this suggests that the major interactions are intradimeric. As described before, the ESR

© 2002 WILEY-VCH Verlag GmbH & Co. KGaA, Weinheim
0947-6539/02/0816-3642 $ 20.00+.50/0 *Chem. Eur. J.* **2002**, *8*, No. 16

studies showed the propagation of weak ferromagnetic interactions within the hydrogen-bonded dimers. Consequently, an additional antiferromagnetic interaction, due to interdimer interactions, competes with the ferromagnetic intradimer interaction, giving rise to the resulting magnetic behavior. Surprisingly, this additional interaction is stronger than the intradimer interaction even when the centers are far apart, and the behavior fitted well to a Curie–Weiss law with $\theta = -4.1$ K. Examination of the crystal structure suggests that the $\pi\cdots\pi$ stacking present between head–tail dimers may be responsible for this strong antiferromagnetic interaction.

The α phase of PTMA exhibits a paramagnetic behavior in the 6–200 K temperature range, and the onset of weak ferromagnetic interactions below 6 K (Figure 11). To confirm

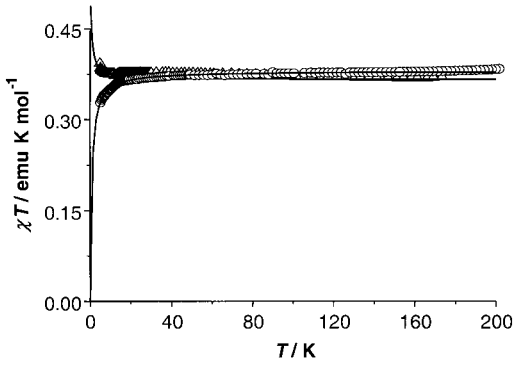

Figure 11. Temperature dependences of the magnetic susceptibility, χ, of polycrystalline samples of α (△) and β (○) phases of radical PTMA which is plotted as χT versus T. Solid lines are the best fit of the experimental data.

this behavior, ESR measurements were performed on an oriented single crystal of the α phase and revealed the same trend. Hence, weak dominant ferromagnetic interactions are present in this phase. The hydrogen-bonded dimers could be responsible, as in the case of NOA, for the appearance of the ferromagnetic interaction within the dimers. As only $Cl\cdots Cl$ contacts are present between the dimers and the distances between them are quite large, it is possible that the dimers behave as magnetically independent species. Therefore, the Bleaney–Bowers equation was used to fit the magnetic data and gave the following exchange coupling constant, $J/k_B = +0.5 \pm 0.1$ K. This value was later confirmed by fitting single-crystal ESR data which gave a similar value, $J/k_B = +1.6 \pm 0.2$ K. In order to validate the ferromagnetic nature of the intradimer interaction, which could not be assessed by ESR measurements in solution, the magnetic data of the β phase was obtained and compared to those of the α phase. Indeed, the β phase differs mainly from the α phase by the absence of such hydrogen-bonded dimers. If these patterns were responsible for the ferromagnetic interaction of the α phase, this ferromagnetic interaction should not be present in the β phase.

The χT product of the β phase of PTMA is plotted against temperature in Figure 11, and shows a continuous decrease as the temperature is lowered. This behavior was fitted to the Curie–Weiss law with a Weiss constant of $\theta = -0.80$ K and indicates of the presence of dominant antiferromagnetic interactions. $Cl\cdots Cl$ contacts may be responsible for this weak antiferromagnetic interaction, as seen in other chlorinated triphenylmethyl radical derivatives.[23] Hence, the comparison of the solid-state magnetic data of both phases clearly showed that the propagation of a ferromagnetic interaction occurs through the hydrogen bond that joins the radicals.

Conclusion

The two open-shell benzoic acid derivatives PTMA and NOA have been used to generate well-defined dimer aggregates in solution, with the aim of investigating whether magnetic exchange occurs at distances longer than 15 Å through noncovalent hydrogen bonds. Such aggregates were found to be present in solution for the NOA radical, and these provided a direct assessment of the resulting ferromagnetic magnetic exchange value. In the case of radical PTMA, aggregates formed through other $Cl\cdots Cl$ and $\pi\cdots\pi$ interactions in solution, as shown by comparison with a reference compound. Indeed, special care must be taken in the study of aggregation and proper reference compounds must be used for each type of radical to ensure that the working concentration does not involve other types of aggregates than those formed through hydrogen bonding. Despite this problem, the exchange interactions were assessed by the consideration of solid-state magnetic behavior. Indeed, the bulkiness of the PTMA radical formed nearly isolated hydrogen-bonded dimers in its α phase. Thus, the exchange interaction through the long-range noncovalent pathway was investigated through solid-state magnetic data and was shown to be ferromagnetic as for NOA. Suppression of this interaction in the β phase, in which dimers were not formed, gave further evidence that the hydrogen-bonded dimers are the species uniquely responsible for this interaction. This magnetic exchange interaction at a long distance is more surprising in this case, since the COOH groups are strongly twisted. Therefore, we have demonstrated that exchange through hydrogen-bonded bridges can occur at a long distance even in the cases of well-delocalized radicals. Even if these noncovalent interactions remain weak, they can play a role in the establishment of ordered magnetic materials when two- and three-dimensional hydrogen-bonded networks are present.

Experimental Section

Materials and methods: Solvents were distilled before use. In particular, THF was dried over sodium/benzophenone, and distilled under Argon. CO_2 gas was dried over concentrated H_2SO_4 and molecular sieves (3 Å). All the reagents were used as received and they were purchased from Aldrich. Thin-layer chromatography (TLC) was performed on aluminum plates coated with Merck Silica gel $60F_{254}$. Microanalyses were performed by the Servei d'Analisi of the Universitat Autònoma de Barcelona. ^1H and ^{13}C NMR spectra were recorded on a Bruker ARX300 spectrometer, FT-IR spectra on a Perkin–Elmer Spectrum One spectrometer, UV-visible spectra on a VARIAN Cary 5 instrument, and the MS spectra on a Jeol JMS-DX300 instrument. The ESR spectra were recorded on X-band Bruker spectrometer (ESP-300E). Temperature was measured by a thermocouple introduced inside the tube, 1.5 cm from the bottom.

 © 2002 WILEY-VCH Verlag GmbH & Co. KGaA, Weinheim 0947-6539/02/0816-3643 $ 20.00+.50/0

Magnetic susceptibility measurements were obtained with a Quantum Design SQUID magnetometer. Crystals were measured on a Nonius KappaCCD diffractometer with an area detector and graphite-monochromized $Mo_{K\alpha}$ radiation.

CCDC 175393 (radical NOA), 175394 (α phase, radical PTMA), and 175395 (β phase, radical PTMA) contain the supplementary crystallographic data for this paper. These data can be obtained free of charge via www.ccdc.cam.ac.uk/conts/retrieving.html (or from the Cambridge Crystallographic Data Centre, 12 Union Road, Cambridge CB2 1EZ, UK; fax: (+44) 1223-336-033; or e-mail: deposit@ccdc.cam.ac.uk)..

1-[*N*-*tert*-Butyl-*N*-(*tert*-butyldimethylsiloxy)amino]-4-benzoic acid: A solution of *tert*-butyllithium (8.8 mL of a 1.7 M solution, 15.0 mmol) was added dropwise to 1-[*N*-*tert*-butyl-*N*-(*tert*-butyldimethylsiloxy)amino]-4-bromobenzene[21] (4.88g, 13.7 mmol) in THF (100 mL) at $-80\,^{\circ}C$. The resulting yellow-orange mixture was stirred at this temperature for 1 h and then allowed to warm slowly to room temperature. The mixture was then cooled to $-30\,^{\circ}C$, and CO_2 was bubbled into the vigorously stirred solution until its consumption ceased. The mixture was then acidified with a 2 M HCl solution until pH = 2. After the usual treatment, removal of the solvents yielded 4.1 g of a cream semisolid which was purified by silica column chromatography (dichloromethane) to give 3.8 g of a white microcrystalline solid. Yield: 85%; ^1H NMR (250 MHz, $CDCl_3$): $\delta = 8.02$ (d, 2H), 7.37 (d, 2H), 1.12 (s, 9H), 0.92 (s, 9H), -0.09 ppm (brs, 6H); MS FAB+ (NBA): *m*/*z* (%): 324 (30) [M^++H]; elemental analysis calcd (%) for $C_{17}H_{29}NO_3Si$: C 63.12, H 9.04, N 4.33, Si 8.68; found C 63.16, H 9.10, N 4.29, Si 8.81.

1-[*N*-*tert*-Butyl-*N*-(hydroxyl)amino]-4-benzoic acid: Hydrofluoric acid (0.17 mL, 22 M) was added to a solution of 1-[*N*-*tert*-butyl-*N*-(*tert*-butyldimethylsiloxy)amino]-4-benzoic acid (1.00 g, 3.0 mmol) in THF (10 mL). The mixture was stirred under inert atmosphere for 1 h and then evaporated under vacuum to give 0.60 g of a white powder. Yield 92%; m.p.: 170 °C (decomp); ^1H NMR (250 MHz, CD_3COCD_3) $\delta = 7.97$ (d, 2H), 7.37 (d, 2H), 1.22 ppm (s, 9H); MS FAB+ (NBA): *m*/*z* (%): 210 [M^++H]; IR (KBr) $\tilde{\nu} = 3246$ (s, br, OH), 2971 (s, CH,*t*Bu), 2650 (s, br, OH), 1686, 1606 (s, s, C=O), 1581 cm^{-1} (m, C=CAr); elemental analysis calcd (%) for $C_{11}H_{15}NO_3$: C 63.14, H 7.23, N 6.69; found C 63.11, H 7.15, N 6.78.

1-[*N*-*tert*-Butyl-*N*-(oxyl)amino]-4-benzoic acid: Lead dioxide (1 g) was added to a solution of 1-[*N*-*tert*-butyl-*N*-(hydroxy)amino]-4-benzoic acid (0.5 g, 2.4 mmol) in ethanol (10 mL). The mixture was vigorously stirred for 1 h and then filtered on a glass frit. Evaporation of the solvent gave 0.55 g of a red solid, which was purified by silica chromatography (dichloromethane/ethylacetate 50:50) to give 0.42 g of a red crystalline powder. Yield 84%; m.p.: 162–167 °C (decomp); MS FAB− (NBA): *m*/*z* (%): 207 (100) [M^- − H]; IR (KBr) $\tilde{\nu} = 3116$ (w, CH,Ar), 2978 (m, CH,*t*Bu), 2667, 2558 (m, m, OH), 1675, 1588 (s, s, C=O), 1563 (m, C=CAr), 1430 (s, δ*t*Bu); elemental analysis calcd (%) for $C_{11}H_{14}NO_3$: C 63.45, H 7.78, N 6.73; found C 63.57, H 6.42, N 6.45.

Acknowledgements

This work was supported by grants from the DGI, Spain (Proyecto no. MAT2000-1388-C03-01), Generalitat de Catalunya (2001SGR-00362), the 3MD Network of the TMR program of the E.U. (Contract ERBFMRXCT 980181), ESF Scientific Programme, and the Region Languedoc-Roussillon (Mobility program). We warmly thank Dr. Carlos J. Gómez-García (Universitat de Valencia) for the magnetic susceptibility measurements.

[1] For a general review of the state-of-art of the field: *Magnetic Properties of Organic Materials* (Ed.: P. M. Lahti), Marcel Dekker, New York, **1999**, and references therein.

[2] a) M. Kinoshita, P. Turek, M. Tamura, K. Nozawa, D.Shiomi, Y. Nakazawa, M. Ishikawa, M. Takahashi, K. Awaga, T. Inabe, Y. Maruyama, *Chem. Lett*. **1991**, 1225; b) M. Tamura, Y. Nakazawa, D. Shiomi, K. Nozawa, Y. Hosokoshi, M. Ishikawa, M. Takahashi, M. Kinoshita, *Chem. Phys. Lett*. **1991**, *186*, 401.

[3] a) G. R. Desiraju, *Crystal Engineering: The Crystal as a Supramolecular Entity: Perspectives in Supramolecular Chemistry*, *Vol. 2*, Wiley, New York, **1996**; b) R. Taylor, O. Kennard, *Acc. Chem. Res.* **1984**, *17*, 320; c) J. A. Zerkowski, C. T. Sete, D. A. Wierda, G. M. Whitesides, *J. Am. Chem. Soc.* **1990**, *112*, 9025; d) M. C. Etter, *Acc. Chem. Res.* **1990**, *23*, 120.

[4] T. Otsuka, T. Okuno, K. Awaga, T. Inabe, *J. Mater. Chem*. **1998**, *8*, 1157.

[5] a) T. Akita, Y. Mazakati, K. Kobayashi, *J. Chem. Soc. Chem. Commun.* **1995**, 1861; b) T. Akita, Y. Mazakati, K. Kobayashi, *Mol. Cryst. Liq. Cryst.* **1997**, *306*, 257; c) Y. Pontillon, T. Akita, A. Grand, K. Kobayashi, E. Lelievre-Berna, J. Pécaut, E. Ressouche, J. Schweitzer, *J. Am. Chem. Soc*. **1999**, *121*, 126.

[6] a) E. Hernandez, M. Mas, E. Molins, C. Rovira, J. Veciana, *Angew. Chem.* **1993**, *105* 919; *Angew. Chem. Int. Ed. Engl.* **1993**, *32*, 882; b) J. Cirujeda, L. E. Ochando, J. M. Amigo, C. Rovira, J. Ruis, J. Veciana, *Angew. Chem*. **1995**, *107*, 99; *Angew. Chem. Int. Ed. Engl.* **1995**, *34*, 55; c) J. Cirujeda, M. Mas, E. Molins, F. Lanfranc de Panthou, J. Laugier, J. G. Park, C. Paulsen, P. Rey, C. Rovira, J. Veciana, *J. Chem. Soc. Chem. Commun*. **1995**, 709; d) J. Cirujeda, E. Hernandez-Gasio, C. Rovira, J.-L. Stanger, P. Turek, J. Veciana, *J. Mater. Chem.* **1995**, *5*, 243; e) J. Veciana, J. Cirujeda, C. Rovira, E. Molins, J. J. Novoa, *J. Phys.* **1996**, 1967; f) T. Sugawara, M. Matsushita, A. Izuoka, N. Wada, N. Takeda, M. Ishikawa, *J. Chem. Soc. Chem. Commun.* **1994**, 1723; f) M. Matsuchida, A. Izuoka, T. Sugawara, T. Kobayashi, N. Wada, N. Takeda, M. Ishikawa, *J. Am. Chem. Soc.* **1997**, *119*, 4369; g) J. Cirujeda, PhD Thesis, Universitat Ramon Llull, **1997**.

[7] T. Akita, K. Kobayashi, *Adv. Mater.* **1997**, *9*, 346.

[8] a) N. Yoshioka, M. Irisawa, Y. Mochizuki, T. Kano, H. Inoue, S. Ohba, *Chem. Lett*. **1997**, 251; b) N. Yoshioka, M. Irisawa, Y. Mochizuki, T. Aoki, H. Inoue, *Mol. Cryst. Liq. Cryst.* **1997**, *306*, 403.

[9] J. R. Ferrer, P. M. Lahti, C. George, G. Antonerra, F. Palacio, *Chem. Mater*. **1999**, *8*, 205.

[10] A. Lang, Y. Pei, L. Ouahab, O. Kahn, *Adv. Mater.* **1996**, *8*, 60.

[11] R. Feher, D. B. Amabilino, K. Wurst, J. Veciana, *Mol. Cryst. Liq. Cryst.* **1999**, *334*, 333.

[12] L. Catala, R. Feher, D. B. Amabilino, K. Wurst, J. Veciana, *Polyhedron*, **2001**, *20*, 1571.

[13] a) F. M. Romero, R. Ziessel, A. De Cian, J. Fischer, P. Turek, *New J. Chem*. **1996**, *20*, 919; b) F. M. Romero, R. Ziessel, M. Drillon, J.-L. Tholence, C. Paulsen, N. Kyritsakas, J. Fischer, *Adv. Mater.* **1996**, *8*, 826; c) F. M. Romero, R. Ziessel, M. Bonnet, Y. Pontillon, E. Ressouche, J. Schweitzer, B. Delley, A. Grand, C. Paulsen, *J. Am. Chem. Soc*. **2000**, *122*, 1298.

[14] a) C. Stroh, F. M. Romero, N. Kyritsakas, L. Catala, P. Turek, R. Ziessel, *J. Mater. Chem*. **1999**, *9*, 875; b) O. Felix, M. W. Hosseini, A. De Cian, J. Fischer, L. Catala, P. Turek, *Tetrahedron Lett.* **1999**, *40*, 2943.

[15] G. A Jeffrey, W. Saenger, *Hydrogen Bonding in Biological Structures*, Springer, Berlin **1994**.

[16] C. Ikeda, N. Nagahara, E. Motegi, N. Yoshioka, H. Inoue, *Chem. Commun.* **1999**, 1759.

[17] K. Inoue, H. Iwamura, *Chem. Phys. Lett*. **1993**, *207*, 551.

[18] N. C. Schiødt, F. Fabrizi de Biani, A. Caneschi, D. Gatteschi, *Inorg. Chim. Acta* **1996**, *248*, 139.

[19] V. Laget, C. Hornick, P. Rabu, M. Drillon, P. Turek, R. Ziessel, *Adv. Mater.* **1998**, *10*, 1024.

[20] a) K. Inoue, H. Iwamura, *Angew. Chem.* **1995**, *107*, 973; *Angew. Chem. Int. Ed. Engl.* **1995**, *34*, 927; b) D. A. Schultz, A. K. Boal, *Mol. Cryst. Liq. Cryst*. **1995**, *272*, 75.

[21] M. Ballester, J. Castañer, J. Riera, A. Ibáñez, J. Pujades, *J. Org. Chem.* **1982**, *47*, 259.

[22] B. Kariuki, C. L. Bauer, K. D. M. Harris, S. J. Teat, *Angew. Chem.* **2000**, *112*, 4659; *Angew. Chem. Int. Ed.* **2000**, *39*, 24, 4485.

[23] a) O. Armet, J. Veciana, C. Rovira, J. Riera, J. Castañer, E. Molins, J. Rius, C. Miravitlles, S. Olivella, J. Brichfeus, *J. Phys. Chem.* **1987**, *91*, 5608; b) J. Sedó, N. Ventosa, M. A. Molins, M. Pons, C. Rovira, J. Veciana, *J. Org. Chem.* **2001**, *66*, 1567.

[24] a) D. A. Shultz, K. P. Gwaltney, H. Lee, J. *Org. Chem.* **1998**, *63*, 769; b) G. Barbarella, A. Rassat, *Bull. Soc. Chim. Fr.* **1969**, 2378.

[25] a) R. Brière, R.-M. Dupeyre, H. Lemaire, C. Morat, A. Rassat, P. Rey, *Bull. Soc. Chim. Fr.* **1965**, 3290; b) J. E. Wertz, J. R. Bolton, *Electron*

 © 2002 WILEY-VCH Verlag GmbH & Co. KGaA, Weinheim 0947-6539/02/0816-3644 $ 20.00+.50/0 *Chem. Eur. J.* **2002**, *8*, No. 16

spin Resonance, Elementary Theory and Practical Applications, **1994**, Chapman and Hall, New York, p. 112.
[26] W. B. Gleason, R. E. Barnett, *J. Am. Chem. Soc.* **1976**, *98*, 2701.
[27] S. S. Eaton, K. M. More, B. M. Sawant, G. R. Eaton, *J. Am. Chem. Soc.* **1983**, *105*, 6560.
[28] A. A. Dubinskii, O. Ya. Grinberg, A. A. Tabachnik, V. P. Ivanoo, E. G. Rozantzev, Ya. S. Lebedev, *Biofizika* **1974**, *19*, 840.
[29] B. Bleaney, K. D. Bowers, *Proc. R. Soc. London Ser. A* **1952**, *214*, 451.
[30] M. Ballester, J. Riera, J. Castañer, C. Badía, J. M. Monsó, *J. Am. Chem. Soc.* **1971**, *93*, 2215.
[31] D. Ruiz-Molina, PhD Thesis, Universitat Autónoma de Barcelona, Spain, **1995**.

Received: December 4, 2001 [F3722]

 © 2002 WILEY-VCH Verlag GmbH & Co. KGaA, Weinheim 0947-6539/02/0816-3645 $ 20.00+.50/0